Tautomerism of Uracil Probed via Infrared Spectroscopy of Singly Hydrated Protonated Uracil

Joost M. Bakker,[†] Rajeev K. Sinha,[‡] Thierry Besson,[‡] Maurizio Brugnara,[‡,§] Paolo Tosi,[§] Jean-Yves Salpin,[||] and Philippe Maître*,[‡]

Laboratoire de Chimie Physique, UMR 8000 CNRS, Faculté des sciences, Université Paris-Sud 11, Bâtiment 350, 91405 Orsay, France, FOM Institute for Plasma Physics Rijnhuizen, Edisonbaan 14, 3439 MN Nieuwegein, The Netherlands, Dipartimento di Fisica, Università di Trento, 38100 Povo Trento, Italy, and Laboratoire d'Analyse et de Modélisation pour la Biologie et l'Environnement, Université d'Evry Val d'Essonne, CNRS, Bâtiment Maupertuis, Boulevard François Mitterrand 91025 Evry, France

Received: July 20, 2008; Revised Manuscript Received: September 24, 2008

Tautomerism of the nucleobase uracil is characterized in the gas phase through IR photodissociation spectroscopy of singly hydrated protonated uracil created with tandem mass spectrometric methods in a commercially available Fourier transform ion cyclotron resonance mass spectrometer. Protonated uracil ions generated by electrospray ionization are re-solvated in a low-pressure collision cell filled with a mixture of water vapor seeded in argon. Their structure is investigated by IR photodissociation spectroscopy in the NH and OH stretching region (2500−3800 cm^{-1}) with a tabletop IR laser source and in the 1000−2000 cm^{-1} range with a free-electron laser. In both regions the IR photodissociation spectrum exhibits well-resolved spectral signatures that point to the presence of two different types of structure for monohydrated protonated uracil, which result from the two lowest-energy tautomers of uracil. Ab initio calculations confirm that no water-catalyzed tautomerization occurs during the re-solvation process, indicating that the two protonated forms of uracil directly originate from the electrospray process.

1. Introduction

Among the molecular bricks of the living world, DNA bases play a key role by establishing noncovalent hydrogen bonds responsible for the encoding and expression of genetic information. In this respect, the rich tautomerism of these DNA bases is of fundamental importance. Uracil, for instance, is found in its canonical structure, a dioxo tautomer, in the Watson−Crick base-pair structure, where it binds to the adenine nucleobase.[1] Alternative tautomeric forms of uracil, however, can be formed upon proton transfer reactions. These different tautomers may be implicated in point mutations, which develop in nucleic acid replication.[2] Acido-basic properties of the nucleobases are of fundamental importance for the strength of internucleic acid hydrogen bonds, which play a role in stabilization of triplex structures[3] and in mutagenic processes.[4]

To obtain information on intrinsic properties such as tautomerism of these biologically important building blocks, it is of particular interest to study molecules isolated from their environment. Following the advent of soft ionization methods such as electrospray[5] and matrix-assisted laser desorption,[6] that allow for facile formation of large ions in the gas phase, the thermochemistry of gas-phase ions derived from biologically important molecules has been studied extensively by tandem mass spectrometry (MS). Although several MS[7] and theoretical[8,9] studies have characterized the gas-phase basicity and proton affinity of the nucleobases, gas-phase structural information is rather scarce. It is therefore clear that direct information on the protonation sites of nucleic bases and on the presence of tautomers in the gas phase is of fundamental importance.

A powerful method to obtain such direct structural information on molecular ions is the combination of tandem mass spectrometry with structure-specific activation techniques. In particular, resonant IR photodissociation spectroscopy allows for a direct probe of the structure of the species under study. The use of free-electron lasers (FELs) as a source of intense, tunable IR radiation has made it possible to perform IR multiple photon dissociation (IR-MPD) spectroscopy of gas-phase molecular ions over a wide spectral range in the mid-IR. The combination of powerful tandem mass spectrometers with FELs has opened up the possibility of multistep tandem mass spectrometry with resonant IR-MPD as a highly structure sensitive activation technique. Fourier transform ion cyclotron resonance (FT-ICR) mass spectrometers, in particular, have been coupled to the CLIO[10,11] and FELIX[12] FELs, and a large variety of molecular ions has been characterized by IR-MPD spectroscopy.

In a previous study, we reported the mid-IR spectra of the protonated nucleobases cytosine, thymine and uracil,[13] formed through electrospray ionization (ESI), recorded with the FEL based at CLIO in Orsay (France). The case of uracil is interesting since its tautomers each provide several potential protonation sites, leading to a multitude of isomeric ions. It was found that the IR-MPD spectrum of protonated uracil in the 1000−1700 cm^{-1} frequency range is in excellent agreement with the calculated IR absorption spectrum of the protonated keto−enol tautomer, which is the lowest energy structure of the system.[9] However, a clear IR-MPD band observed at 1800 cm^{-1} could not be interpreted by considering only the protonated keto−enol tautomer. An IR-MPD band in this frequency range is typically the signature of a CO stretching vibration and it was proposed that this could be due to the presence of a protonated diketo

* To whom correspondence should be addressed: tel +33-1-69-15-74-63; fax +33-1-69-15-61-88; e-mail philippe.maitre@u-psud.fr.
[†] FOM Institute for Plasma Physics Rijnhuizen.
[‡] Université Paris-Sud 11.
[§] Università di Trento.
[||] Université d'Evry Val d'Essonne.

10.1021/jp806396t CCC: $40.75
Published on Web 11/11/2008

tautomer. The proposition of coexistence of two tautomers under our experimental conditions was further strengthened by quantum chemical calculations, which predict the two tautomeric forms to be energetically close.[13] Although the evidence is rather convincing, additional spectroscopic information in the range between 2000 and 4000 cm^{-1} could have reinforced the present interpretation. In this spectral range, highly characteristic NH and OH stretching vibrations are found, which form direct evidence for the presence of protonated canonical dioxo and enolic tautomers. Unfortunately, this spectral range is inaccessible with the CLIO FEL. An alternative source of IR radiation, a tabletop optical parametric oscillator/amplifier (OPO/OPA) combination, does cover the spectral range, but the light produced is not sufficiently intense to induce fragmentation in strongly bound ionic systems.

To circumvent this problem, we here present IR spectra of the monohydrated protonated uracil. The relative weakness of the protonated uracil−water bond allows for an efficient IR-induced photodissociation. At the same time, it will be shown that the stepwise addition of water molecules to bare uracil ions formed under ESI conditions does not influence their tautomeric form, as this change requires an interconversion with a rather high internal energy barrier.

To achieve this, ESI conditions are optimized to produce bare protonated uracil. The uracil ions are then complexed with water molecules in a collision cell containing low-pressure argon seeded with water vapor. The IR spectrum of monohydrated protonated uracil is recorded with the CLIO FEL in the mid-IR spectral range and with the OPO/OPA laser system in the 2500−4000 cm^{-1} spectral range. Both experiments are performed under the same experimental conditions in a 7 T FT-ICR mass spectrometer.[11] Analysis of the IR-MPD spectrum indeed suggests that two classes of structures are involved. A comparison with calculated IR absorption spectra of structural isomers of the ions suggests that the spectra recorded correspond to those of monohydrated protonated diketo and keto−enol tautomers of uracil.

2. Experimental and Computational Details

IR-MPD spectroscopy of hydrated protonated uracil ions is performed by use of a 7 T FT-ICR mass spectrometer (Bruker, Apex Qe) into which IR light produced by one of two IR lasers is coupled. As the detailed layout of this experimental apparatus is described elsewhere,[11] only a brief overview is given here.

Protonated uracil ions are prepared in an ESI source by introducing a 10^{-4} M aqueous solution of the nucleobase in water (purified with a Milli-Q water purification system) into the source using direct infusion with a syringe pump. Critical ESI conditions used are a flow rate of 3 μL/min, a spray voltage of 3500 V, and a capillary temperature of 200 °C.

The most important feature of the mass spectrometer for the present study is its quadrupole−hexapole interface between the electrospray source and the ICR cell. The bias voltage and RF amplitude of the quadrupole are adjusted to selectively transmit protonated uracil. Mass-selected ions are then trapped in a ∼5 cm long hexapole ion trap contained within a collision cell where ions normally are collisionally cooled with a flow of high-purity argon buffer gas. In the present study, water vapor is seeded in the argon gas flow. Ions are typically stored in the ion trap over periods of ∼50 ms, leading to solvation of some ∼60% of the protonated uracil ions. Ions are then pulse-extracted toward the ICR cell, where mass selection of monosolvated protonated uracil is performed. They are then irradiated with IR light, after which the resulting ions are mass-analyzed.

If the IR light is in resonance with an IR-active vibrational mode of molecular ions stored in the ICR cell, IR photons can be absorbed by the ions and the sequential absorption of several IR photons can lead to fragmentation of the mass-selected ions. This photofragmentation, which is the result of a multiple photon absorption process, is often termed infrared multiple photon dissociation (IR-MPD). By monitoring the number of detected ions in the precursor mass channel and that in the fragment mass channels while the frequency of the IR light is varied, an IR-MPD spectrum is obtained. For each wavelength, the mass spectrum is the Fourier transform of a time-domain transient averaged 5 times.

For the present study, two sources of IR light are used. The 2500−4000 cm^{-1} wavenumber range is explored by use of an IR optical parametric oscillator/amplifier (OPO/OPA) system (LaserVision), pumped by a 25 Hz Nd:YAG laser (Innolas Spitlight 600, 550 mJ/pulse, 1064 nm, 4−6 ns pulse duration). In the presently covered wavenumber range, the typical output energy slowly decreases from ∼12 mJ/pulse at 3600 cm^{-1} to 3.5 mJ at 2500 cm^{-1} with a spectral bandwidth of ∼5 cm^{-1}. For the 1000−2000 cm^{-1} spectral range, the CLIO FEL is used.[14] The FEL produces IR light in so-called macropulses at a repetition rate of 25 Hz. Each macropulse consists of a pulse train of picosecond duration light pulses. The spectral bandwidth is ∼0.5% of the central frequency, thus ranging from ∼5 cm^{-1} at 1000 cm^{-1} to ∼10 cm^{-1} at 2000 cm^{-1}. Typical macropulse energies are 40 mJ, but to avoid spectral saturation in the present study, the IR intensity is reduced via fixed-value attenuators and the resulting macropulse energy is ∼4 mJ. For both lasers, the IR laser beam is steered into the FT-ICR along the axis of the magnetic trapping field and loosely focused by use of a spherical mirror with a 2-m focal distance. The light beam has a nearly constant diameter throughout the ICR cell region.

To aid in interpretation of the recorded spectra, density functional theory (DFT) calculations are performed to obtain the absorption spectra of several possible structures of protonated uracil−water. All calculations are performed with the Gaussian03 program suite[15] using the B3LYP hybrid density functional. Kohn−Sham orbitals are expanded in the 6-311++G(3df,2p) Gaussian basis set, except for determination of the potential energy profile associated with the water-catalyzed tautomerization, for which the reduced 6-31++G(d,p) basis set was chosen.

Harmonic vibrational frequencies are determined. In order to facilitate the comparison of IR-MPD spectra with calculated IR absorption spectra, each calculated band is convoluted, with the assumption of a Lorentzian profile. The width (fwhm) is 20 cm^{-1} (10 cm^{-1}) in the 1000−2000 cm^{-1} (2500−3800 cm^{-1}) frequency range.

3. Results

3.1. Photodissociation Spectra. Multiple collisions of protonated uracil (UH^+) with the water/argon buffer gas in the hexapole collision cell over a time period of 50 ms leads to a substantial fraction of the uracil ions clustered with one water molecule ($UH^+ \cdot OH_2$). Interestingly, larger cluster sizes are not observed in substantial amounts. After the ejection of masses other than that of the singly hydrated uracil ions in the ICR cell, m/z 131 ions are irradiated for 150 ms. Mass spectra recorded after irradiation at two different wavenumbers are shown in Figure 1. In Figure 1a, loss of the water molecule is clearly observed after irradiation with light at 3548 cm^{-1}. The mass spectrum depicted in Figure 1b is typical for what is observed when the IR laser is off-resonance. The small intensity at m/z 113 present here is most likely due to thermal dissociation, as it is also observed when no IR laser is present.

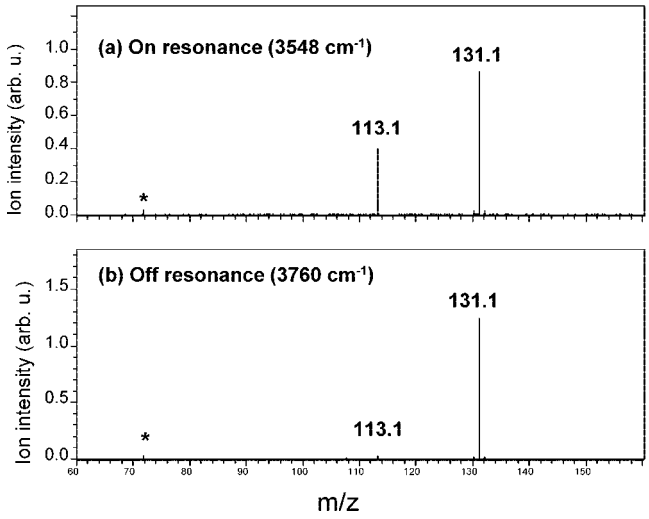

Figure 1. Mass spectra recorded after the irradiation of precursor ions at (a) 3548 and (b) 3760 cm^{-1}, where the precursor and fragment ions are $UH^+ \cdot OH_2$ (*m/z* 131.1) and UH^+ (*m/z* 113.1), respectively. The peak at *m/z* 72 (*) is due to electrical interference picked up by the detection plates of the ICR cell.

A maximum photofragmentation yield of ~73% is observed when the IR laser is tuned to 3425 cm^{-1}. It should be noted that even under these circumstances no photofragments other than the bare protonated uracil (*m/z* 113) are observed on resonance with an IR-active vibrational mode of $UH^+ \cdot OH_2$. Considering that the irradiation time of 150 ms comprises three IR laser pulses, a sequential IR-induced photofragmentation of the UH^+ photofragment itself (*m/z* 113) could have been expected since solvated and nonsolvated protonated uracil are likely to share some spectral features. In order to confirm that bare UH^+ cannot be fragmented upon resonant IR absorption in the experimental time window, an additional experiment is performed where mass-selected UH^+ (*m/z* 113) ions were irradiated by the IR laser. Even after irradiation times exceeding 2 s, no photofragmentation of protonated uracil was observed in the 3500 cm^{-1} region where the output energy of the IR OPO/OPA system is maximal (~12 mJ) and where the most intense spectral modes are expected.

3.2. IR Spectra in the 2600−3800 cm^{-1} Spectral Range. If the wavelength is varied while the number of precursor and fragment ions is recorded, the IR spectrum is obtained. It is typically expressed in the IR photodissociation efficiency defined as $-\ln [I_P/(I_P + I_F)]$,[16] where I_P and I_F are the intensities of the precursor ions and the fragment ions, respectively. The resulting IR spectrum of $UH^+ \cdot H_2O$ ions recorded in the 2600−3800 cm^{-1} spectral range is shown in Figure 2. As can be seen in this figure, four clear IR bands with bandwidths (fwhm) of ~25−30 cm^{-1} are observed in the 3200−3800 cm^{-1} range, with band maxima at 3425, 3556, 3625, and 3702 cm^{-1}. The strongest, at 3425 cm^{-1}, has a distinct shoulder on the red, which is attributed to a fifth resonance at 3390 cm^{-1}. The frequencies of these IR bands typically fall in the spectral range where one would expect NH and OH stretches. Below 3200 cm^{-1}, a broad but distinct resonance structure can be discerned with a maximum at ~2920 cm^{-1}. This broad feature, a sixth resonance, could be the signature of a red-shifted X−H (X = N, O) stretching vibration where the hydrogen is involved in a hydrogen bond.

4. Discussion

4.1. Optimized Structures of Monohydrated Protonated Uracil. An analysis of the experimental IR spectrum can be supported by comparison with calculated IR absorption spectra

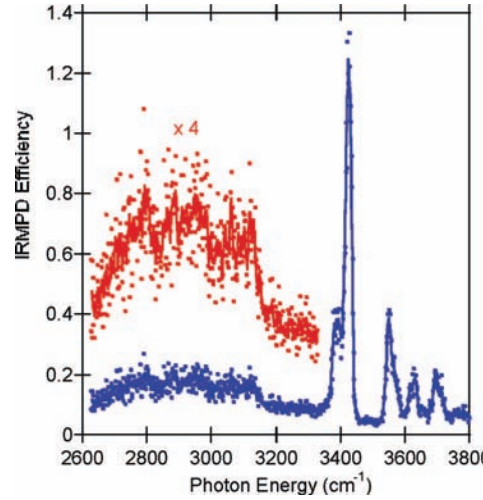

Figure 2. Infrared photodissociation spectrum of $UH^+ \cdot OH_2$ (*m/z* 131.1) ions recorded with the OPO/OPA laser system. Line spectrum corresponds to a smoothing of the experimental data (squares).

for the possible structures of $UH^+ \cdot OH_2$. A starting point for the search for $UH^+ \cdot OH_2$ structures is formed by the known low-energy structures for UH^+.[9,13] Similar to a recent study of UH^+ solvated by ammonia,[17] the hydrated structures considered here are those resulting from the addition of water to the two lowest energy structures of UH^+. In Scheme 1 the relationships between the different low-energy structures found for $UH^+ \cdot OH_2$ and the neutral uracil tautomers are indicated.

Protonation of the canonical diketo form of uracil leads to the least stable of the UH^+ structures in which the proton is bound to one of the carbonyls. Interestingly, the addition of water to this structure yields the most stable of all hydrated structures, the one here labeled U(DK)H^+_W. Two hydrated structures that are slightly higher in energy result from the solvation of the most stable structure of UH^+. This most stable structure of UH^+ (by 3.8 kJ/mol at the present level of theory) originates from the protonation of neutral keto−enol and can be seen as the resonance of two Kekule structures. The hydrated structures U(KE)H^+_Wa and U(KE)H^+_Wb correspond to addition of the water molecule on the formal location of the proton in each of the two, and they have relative energies 7.2 and 13.1 kJ/mol higher than that for structure U(DK)H^+_W, respectively. The fully optimized geometries of the lowest-energy hydrated structures U(DK)H^+_W, U(KE)H^+_Wa, and U(KE)H^+_Wb are depicted in Figure 3, with their corresponding bond lengths and relative energies.

The structures and energetics of $UH^+ \cdot OH_2$ can be compared to those of $UH^+ \cdot NH_3$, proposed in a recent high-pressure mass spectrometric study.[17] The same energy ordering was found when UH^+ was solvated by ammonia.[17] Similar to the present case, the lowest energy structure of $UH^+ \cdot NH_3$ corresponds to the protonated canonical form of uracil [U(DK)H^+], with NH_3 bound to the proton. Upon geometry optimization of the clusters formed by UH^+ and NH_3, a partial proton transfer from uracil to NH_3 was found. As can be seen in Figure 3, no such proton transfer occurs for $UH^+ \cdot OH_2$, where the C═O−H^+ distance is typically on the order of 1.01 Å and the H_2O−H^+ bond length is 1.58 Å. This result may not be surprising when it is considered that the proton affinity of water is significantly lower than that of ammonia. It should be stressed, however, that a partial proton transfer is found for uracil−NH_3[17] even though the proton affinity for uracil is larger than for NH_3.[18]

The minimum number of absorbed IR photons required for fragmentation of $UH^+ \cdot OH_2$ into UH^+ and water can be

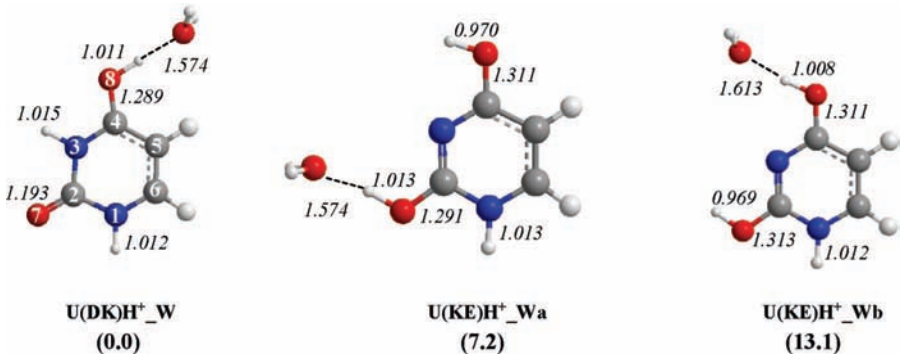

Figure 3. Optimized (C_s symmetry) structures of monohydrated protonated uracyl ($UH^+ \cdot OH_2$) at the B3LYP/6-311++G** level of theory. Relatives 0 K energies (shown in parentheses) are in kilojoules per mole; bond lengths are in angstroms.

SCHEME 1

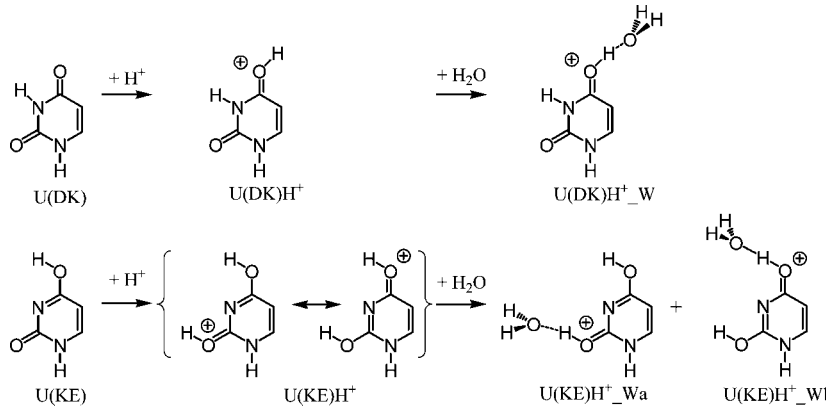

estimated from the calculated binding energies of structures $U(DK)H^+$_W, $U(KE)H^+$_Wa, and $U(KE)H^+$_Wb. With the lowest-energy structure of UH^+ as a reference, the 0 K binding energy of structure $U(DK)H^+$_W is 70.2 kJ/mol at the B3LYP/6-311++G** level of theory. The difference in free energies at 298 K is 36.1 kJ/mol. In the frequency range explored with the relatively low-intensity OPO/OPA laser, the absorption of one or two IR photons is thus sufficient to overcome the lowest energy fragmentation threshold for $UH^+ \cdot OH_2$ ions.

4.2. NH and OH Stretching Band Assignment. It is interesting to note that the number of experimentally observed resonances cannot be accounted for by fundamental vibrations of one single structure of $UH^+ \cdot OH_2$. Each of the $UH^+ \cdot OH_2$ structures discussed above has five X−H (X = N or O) groups, whereas in the experimental spectrum clearly six resonances have been observed. It is thus not unlikely that the observed IR-MPD spectrum is due to a mixture of different structures coexisting in the ICR cell.

To aid in interpretation of the experimental spectra, the calculated IR spectra for the three structures discussed above are given in Figure 4. In order to facilitate the comparison with the experimental IR photodissociation spectrum, each calculated IR absorption band is convoluted by a Lorentzian function with a width (fwhm) of 10 cm^{-1}. It can be seen in Figure 4 that the three calculated IR absorption spectra have several common features. At low wavenumber, each spectrum exhibits a strong calculated absorption feature (at 2799, 2880, and 2781 cm^{-1} for structures $U(DK)H^+$_W, $U(KE)H^+$_Wa, and $U(KE)H^+$_Wb, respectively). For each structure, the corresponding normal mode is the stretching vibration of the OH involved as a donor in the hydrogen bond with water. It is likely that the broad feature centered at 2919 cm^{-1} observed in the IR spectrum (Figure 4) can be assigned to this red-shifted OH stretch. Previously, such simultaneous red shifts and broadening effects of stretching vibrations of X−H (X = N, O) involved in a hydrogen bond have been observed for water-solvated clusters[19] or solvated amino acids.[20]

On the blue side of the IR spectrum, two IR absorption features characteristic for water OH stretches are found. The symmetric OH stretching vibrations are calculated to lie at 3619, 3631, and 3631 cm^{-1} for structures $U(DK)H^+$_W, $U(KE)H^+$_Wa, and $U(KE)H^+$_Wb, respectively. The asymmetric OH stretching vibrations are predicted at slightly higher frequencies, at 3703, 3719, and 3718 cm^{-1}. Based on the rather small differences in calculated frequencies and intensities of the water OH stretching vibrations for the different structures and the favorable comparison between experimental and calculated IR spectra in this region, it seems reasonable to assign the two highest frequency bands (D and E in Figure 4) observed at 3625 and 3702 cm^{-1} to the symmetric and asymmetric OH stretching vibrations of water, respectively. It is interesting to note that although the calculated IR intensity of the symmetric water OH stretch is approximately 3 times lower than that of the asymmetric stretch (calculated intensities are 50 and 150 km/mol, respectively), the observed IR-MPD efficiencies for these vibrational modes are approximately equal. Similar observations were made for water-solvated clusters, for which photodissociation on resonance with the asymmetric water OH stretch has always been observed to be relatively small. It was recently proposed that the low photodissociation efficiency observed for the water OH asymmetric stretch could be due to an inefficient intramolecular vibrational redistribution (IVR) of the energy from this excited vibrational mode to the bath of vibrational modes of the ion.[21]

The vibrational features observed at bands B and C provide the most valuable information for structural assignment. As can

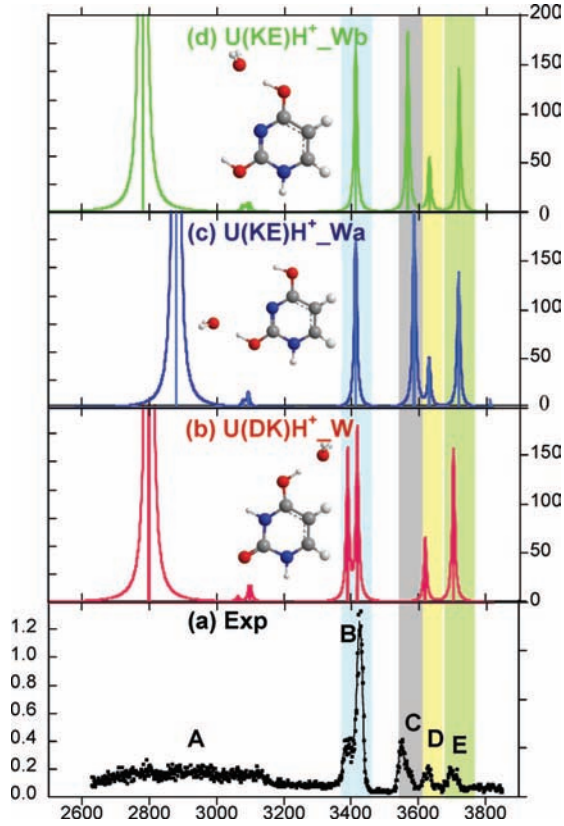

Figure 4. Infrared spectra of monohydrated protonated uracil ($UH^+ \cdot OH_2$) in the 2500−3800 cm^{-1} spectral range. (a) Experimental spectrum; ordinate (left axis) is the photodissociation efficiency. (b−d) Calculated (B3LYP/6-311++G** level of theory) IR absorption spectra of structures (b) $U(DK)H^+$_W, (c) $U(KE)H^+$_Wa, and (d) $U(KE)H^+$_Wb. Calculated intensities (right axis) are given in kilometers per mole. Each IR absorption band is convoluted by a Lorentzian profile (fwhm = 10 cm^{-1}). Scaling factor is 0.955.

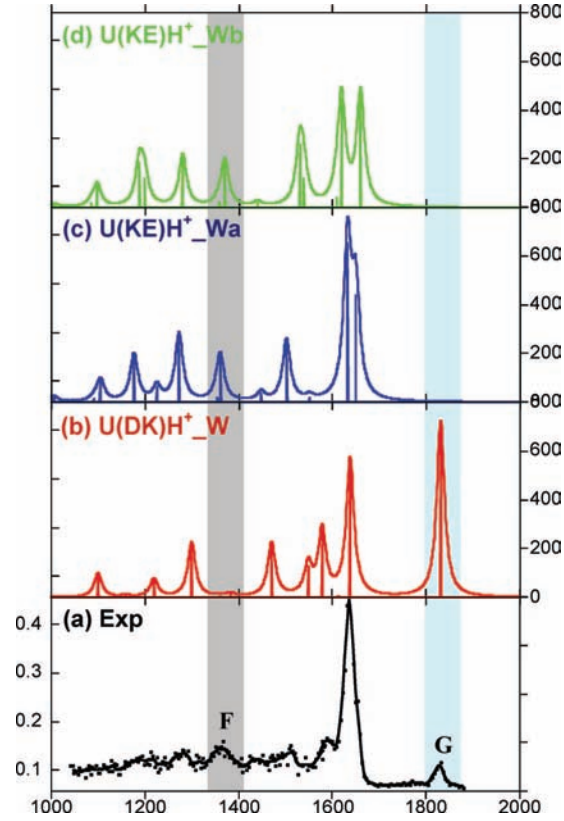

Figure 5. Infrared spectra of monohydrated protonated uracil ($UH^+ \cdot OH_2$) in the 1000−2000 cm^{-1} spectral range recorded with the CLIO IR FEL. (a) Experimental spectrum; ordinate (left axis) is the photodissociation efficiency. (b−d) Calculated (B3LYP/6-311++G** level of theory) IR absorption spectra of structures (b) $U(DK)H^+$_W, (c) $U(KE)H^+$_Wa, and (d) $U(KE)H^+$_Wb. Calculated intensities absorption band is convoluted by a Lorentzian profile (fwhm = 20 cm^{-1}). Scaling factor is 0.98.

be seen in Figure 4, the position of band C (3556 cm^{-1}) nicely matches with the IR absorption band associated with the calculated free OH stretching vibrations of structures $U(KE)H^+$_Wa and $U(KE)H^+$_Wb at 3586 and 3567 cm^{-1}, respectively. Since structure $U(DK)H^+$_W does not display any IR resonance in this wavenumber range, the observation of band C suggests that $U(KE)H^+$_Wa or $U(KE)H^+$_Wb, or a mixture of these structures, is formed under current experimental conditions.

The strongest observed band in this spectral range is band B, which appears to consist of two resonances: the maximum at 3425 cm^{-1} and a red-shifted shoulder at 3390 cm^{-1}. For all calculated structures, IR-active normal modes in the spectral region of band B are free NH stretching vibrations. The free NH stretching vibrations of structures $U(KE)H^+$_Wa and $U(KE)H^+$_Wb are predicted at almost identical frequencies (3412 and 3413 cm^{-1}). Structure $U(DK)H^+$_W has two free NH bonds, for which one calculated at 3417 cm^{-1} has a frequency very similar to those of the free NH stretching vibrations of structures $U(KE)H^+$_Wa and $U(KE)H^+$_Wb. The second free NH stretching vibration for structure $U(DK)H^+$_W is calculated at 3389 cm^{-1}. Interestingly, the frequency difference between the two calculated NH stretching modes for this structure, 28 cm^{-1}, is quite similar to the observed frequency difference between the maximum and the shoulder of band B, 35 cm^{-1}. From this it is inferred that the shape of band B is the signature of the presence of ions with structure $U(DK)H^+$_W under our experimental conditions. The fact that all three structures [$U(DK)H^+$_W, $U(KE)H^+$_Wa, and $U(KE)H^+$_Wb] have a free N(1)_-H stretching mode (see Figure 3 for atom numbering) within a narrow frequency range (3412−3417 cm^{-1}) suggests an assignment of the maximum of band B to that stretching mode in multiple isomers [$U(DK)H^+$_W, $U(KE)H^+$_Wa, and $U(KE)H^+$_Wb]. The shoulder of band B at 3390 cm^{-1} is then assigned to the N(3)−H stretching vibration in $U(DK)H^+$_W only.

4.3. Mid-IR (1000−2000 cm^{-1}) Spectrum: Further Evidence for Two Coexisting Tautomers. Additional evidence for the simultaneous formation of isomers $U(DK)H^+$_W, $U(KE)H^+$_Wa, and $U(KE)H^+$_Wb under our experimental conditions can be found by recording the IR-MPD spectrum in the 1000−2000 cm^{-1} spectral range with the IR light produced by the CLIO FEL. The resulting spectrum is shown in Figure 5 together with the calculated IR absorption spectra of structures $U(DK)H^+$_W, $U(KE)H^+$_Wa, and $U(KE)H^+$_Wb.

It can be seen in Figure 5 that the experimental IR-MPD spectrum of $UH^+ \cdot OH_2$ is well structured, with the strongest feature observed at 1636 cm^{-1}. Interestingly, the maximum IR-MPD signal was also obtained at about the same frequency in the case of UH^+.[13] The three structures $U(DK)H^+$_W, $U(KE)H^+$_Wa, and $U(KE)H^+$_Wb all have particularly strong IR absorption bands in the 1620−1659 cm^{-1} frequency range. The associated normal modes are ring deformation with a strong component on the C(5)−C(6) stretch. The strongest photodissociation feature observed at 1636 cm^{-1} for $UH^+ \cdot OH_2$ is thus not conclusive and could be the result of the photofragmentation

of each single structure, or a mixture of the three structures, of $UH^+ \cdot OH_2$ proposed above.

A clear-cut IR signature for the presence of the hydrated diketo tautomer of UH^+, however, can be found. As in the case of UH^+,[13] a band is observed in the 1800 cm^{-1} frequency range (band G in Figure 5) where a CO stretching mode is the only expected IR-active mode. The observed frequency (1828 cm^{-1}) nicely matches with the calculated CO stretching frequency for structure U(DK)H^+_W; that is, the monohydrated protonated diketo tautomer of uracil. The present results on $UH^+ \cdot OH_2$ thus support our earlier conclusion that a fraction of the UH^+ ions formed under our experimental conditions correspond to the protonated diketo tautomer of uracil.[13]

Evidence for the formation of singly hydrated protonated keto−enol tautomer of uracil [that is, structures U(KE)H^+_Wa and/or U(KE)H^+_Wb] can also be found in the spectral range below 1600 cm^{-1}. As can be seen in Figure 5, band F observed at 1362 cm^{-1} nicely matches with an IR absorption band of structure U(KE)H^+_Wa (1360 cm^{-1}) or U(KE)H^+_Wb (1370 cm^{-1}). On the other hand, structure U(DK)H^+_W of $UH^+ \cdot OH_2$ does not display any significant IR-active mode in the 1299−1470 cm^{-1} frequency range. From this, it is inferred that the band observed at 1362 cm^{-1} is a signature of the formation of structure U(KE)H^+_Wa or U(KE)H^+_Wb, or a mixture of both, under our experimental conditions. The IR-active vibrations of U(KE)H^+_Wa (1360 cm^{-1}) and U(KE)H^+_Wb (1370 cm^{-1}) are associated with bending of the C−O−H group involved in the hydrogen bond with water. The frequency of this vibration for structure U(DK)H^+_W is calculated to be lower (1272 cm^{-1}). The blue shift of this vibration in the keto−enol structures could be attributed to the interaction between the C−O−H hydrogen and the N(3), which is not involved in the diketo structure due to the orientation of the H-bound COH (see Figure 3).

4.4. Proton Transfer in Protonated Uracil. The IR signature of the two monohydrated protonated tautomers of uracil can be unambiguously distinguished in the two IR photodissociation spectra discussed above. In our recent study on protonated uracil, spectroscopic evidence for the coexistence of two protonated tautomers of uracil UH^+ were also given, and it was proposed that these two structures were formed under electrospray conditions.[13] In the present experiment, $UH^+ \cdot OH_2$ ions are formed through multiple collisions between mass-selected UH^+ ions and water. These collisions occur in a pressurized collision cell where water is seeded in argon at an estimated pressure of 10^{-3} mbar. It is important to evaluate whether tautomerization can occur during this microsolvation process.

Unimolecular proton transfer in protonated uracil has been shown to be associated with a large activation barrier. At the B3LYP/6-311++G(3df,2p)//B3LYP/6-31++G(d,p) level of theory, the energy barrier for interconversion of U(DK)H^+ into the more stable U(KE)H^+ tautomer is 164.7 kJ/mol, where the rate-limiting step is the 1,3 proton transfer from cyclic N(3) to exocyclic O(7).[13] However, upon addition of a base, such a 1,3 proton transfer can be efficiently catalyzed.[22] This has been demonstrated for the addition of NH_3 to protonated thymine, where the activation barrier is lowered by about 125 kJ/mol.[17]

The potential energy profile for water-catalyzed tautomerization of protonated uracil is given in Figure 6. Due to difficulties in optimizing the transition-state structures at the 6-311++G(3df,2p) level of theory, the 298 K Gibbs energies given in Figure 6 were obtained at the B3LYP/6-31++G(d,p) level of theory, which is the reason for small discrepancies in the relative energies of $UH^+ \cdot OH_2$ compared to those given in Figure 3, which are obtained at the B3LYP/6-311++G(3df,2p) level of theory.

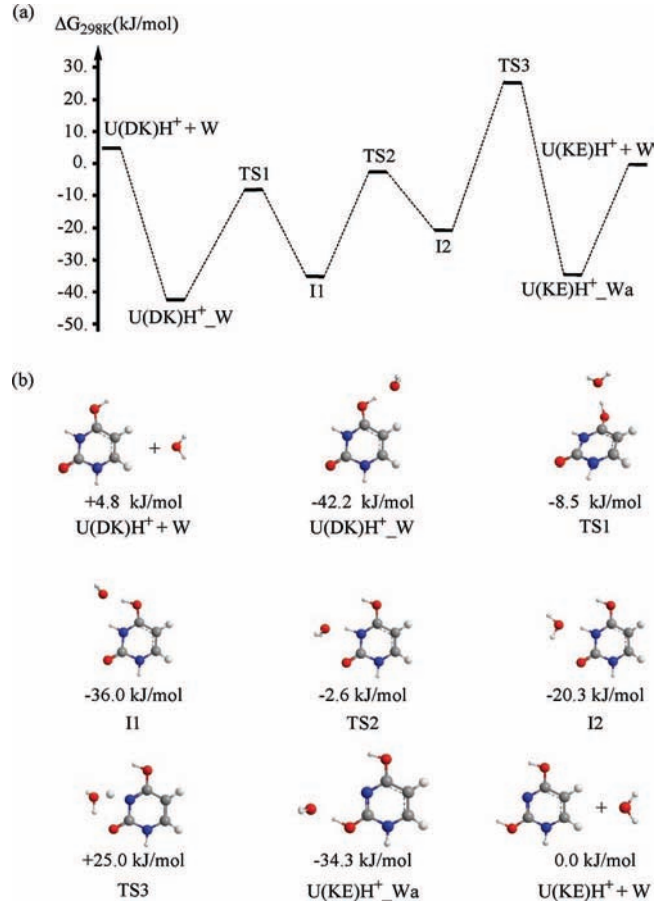

Figure 6. Potential energy profile associated with the water-catalyzed 1,3 proton transfer converting U(DK)H^+_W into U(KE)H^+_Wa determined at the B3LYP/6-31+G** level of theory. (a) 298 K Gibbs energies. Energies are given relative to the protonated keto−enol uracil [U(KE)H^+] + water asymptote. (b) Optimized structures involved in the tautomerization.

As found by Wu and McMahon[17] for the reaction involving UH^+ and NH_3, tautomerization of U(DK)H^+_W into U(KE)H^+_W involves two intermediates (I1 and I2 in Figure 6): starting from U(DK)H^+_W, a rotation about the exocylic C−O(8) is followed by a transfer of water from exocyclic O(8)H to N(3)H.

In contrast to the case of ammonia,[17] the transition state (TS3, see Figure 6) associated with the water-catalyzed 1,3 proton transfer is high in energy. Relative to the U(DK)H^+_W isomer, the 298 K Gibbs free energy barrier is 69.5 kJ/mol. It is thus significantly lowered by the addition of water, but significantly less than upon addition of ammonia.[17] This difference is expected since TS3 involves a partial proton transfer from uracil to the base, and the proton affinity of water is significantly lower than the one of ammonia (691 and 853.6 kJ/mol, respectively).[18] Considering that our calculated value for the difference in proton affinity of uracil and water is only slightly lower than the experimental value (181.3 and 181.7 kJ/mol, respectively), the calculated barrier height associated with TS3 (Figure 6) can be taken with confidence.

Energies reported in Figure 6 are given relative to the lowest energy dissociation channel leading to U(KE)H^+ + OH_2. As can be seen in Figure 6, TS3 associated with the rate-limiting step lies 34.5 kJ/mol above U(KE)H^+ + OH_2. On the basis of these results, one may conclude that water-catalyzed tautomer-

ization of protonated uracil is unlikely to occur during the resolvation step within the pressurized collision cell. It is rather suggested that the two types of isomers characterized by their spectroscopic signatures are formed through microsolvation of two tautomeric forms of protonated uracil, $U(DK)H^+$ and $U(KE)H^+$, formed by electrospray ionization.

5. Summary and Outlook

Gas-phase IR photodissociation spectra of singly hydrated protonated uracil, $UH^+ \cdot OH_2$, have been recorded in the 1000−2000 and 2500−3800 cm^{-1} spectral ranges. In both regions, the IR spectrum exhibits well-resolved spectral features that indicate the presence of two types of structures for $UH^+ \cdot OH_2$. The IR photodissociation spectrum in the 2500−3800 cm^{-1} region clearly displays six resonances, whereas each of the $UH^+ \cdot OH_2$ structures can only display five fundamental vibrational modes in this spectral range.

Ab initio calculations identify three possible low-energy structures, which are the result of solvation of the two lowest-energy structures of protonated uracil: a protonated diketo and a protonated keto−enol tautomer.

Comparison with the calculated IR absorption spectra of the three lowest-energy structures of $UH^+ \cdot OH_2$ shows that a band observed at 3556 cm^{-1} is the signature of a protonated keto−enol tautomer of uracil, while a doublet structure in the NH stretching range (3389 cm^{-1} and 3412−3417 cm^{-1}) provides evidence for the simultaneous formation of the protonated keto−enol tautomer under our experimental conditions. These conclusions are further supported by the IR photodissociation spectrum recorded at 1000−2000 cm^{-1} via IR-FEL. Solvation of the protonated diketo tautomer is unambiguously characterized by a band observed in the CO stretching region (1828 cm^{-1}). From a comparison between the calculated IR absorption spectra, a band observed at 1362 cm^{-1} clearly points at the presence of structures resulting from hydration of the protonated keto−enol tautomer.

It would be particularly interesting to record the IR spectrum of a single conformer. For gas-phase ions such conformation-specific spectroscopy could be performed by different schemes. For larger protonated peptides, a selection based on the shape of the system could be performed with an ion mobility drift tube upstream of the ion trap. UV-based double-resonance (IR-UV) spectroscopic techniques have been successfully applied by the Rizzo group,[23] who have obtained exciting results for systems ranging from protonated amino acids to medium-sized polypeptides. A third alternative would be to use IR-IR double resonance spectroscopy, where a first scanning IR laser is fired before a second conformer-specific fixed frequency probe laser. Any fragments created by the first laser (the burn laser) are removed by mass isolation before the probe laser is fired. The probe signal will then be depleted when the burn laser is in resonance with a vibration that belongs to the same conformer. This method is currently being pursued by Johnson and co-workers,[24] who implement the tandem mass spectrometry procedure with a double-reflectron time-of-flight configuration. The capabilities of our present experiment make it a logical step to evaluate the possibilities of such double-resonance techniques.

Another important issue is to improve the spectroscopic sensitivity, especially for the use of relatively low-power IR OPO/OPA laser systems in IR photodissociation spectroscopy of gas-phase ions. The aforementioned IR-UV double-resonance technique has been shown to be particularly sensitive. A good alternative is to tag the molecular ions of interest with weakly bound rare gas atoms, as demonstrated by the recent IR spectra recorded in the fingerprint spectral range by use of pulse power tabletop laser systems.[25] By use of tandem mass spectrometers such as an FT-ICR, the absorption of an IR photon can also be probed by monitoring the rate of an IR-induced ion−molecule reaction. Provided that the intrinsic endothermicity of the reaction is on the order of magnitude of the photon energy, a greater spectroscopic sensitivity can be anticipated than when absorption of multiple photons is needed to induce fragmentation. This approach has already successfully been used with a 22-pole ion trap within a relatively high pressure collision cell.[26] Preliminary results indicate that this approach can also been used within the ICR cell at low pressure.[27]

Acknowledgment. We gratefully acknowledge the European Commission for a generous grant associated with the EPITOPES (Electron Plus Infrared TO Probe and Elucidate Structures, EC Project 15637) funded through the NEST (New and Emerging Science and Technology) program of the 6th framework program. M.B. thanks the Fondazione Trentino Università for supporting his stay in Orsay.

References and Notes

(1) Watson, J. D.; Crick, F. H. *Nature* **1953**, *171*, 964.

(2) (a) Topal, M. D.; Fresco, J. R. *Nature* **1976**, *263*, 285. (b) Sowers, L. C.; Fazakerley, G. V.; Eritja, R.; Kaplan, B. E.; Goodman, M. F. *Proc. Natl. Acad. Sci. U.S.A.* **1986**, *83*, 5434.

(3) Frankkamenetskii, M. D.; Mirkin, S. M. *Annu. Rev. Biochem.* **1995**, *64*, 65.

(4) Sinden, R. R. *DNA Structure and Function*, 1st ed.; Academic Press: San Diego, CA, 1994.

(5) Fenn, J. B.; Mann, M.; Meng, C. K.; Wong, S. F.; Whitehouse, C. M. *Science* **1989**, *246*, 64.

(6) Karas, M.; Hillenkamp, F. *Anal. Chem.* **1988**, *60*, 2299.

(7) (a) Wilson, M. S.; McCloskey, J. A. *J. Am. Chem. Soc.* **1975**, *97*, 3436. (b) Meotner, M. *J. Am. Chem. Soc.* **1979**, *101*, 2396. (c) Greco, F.; Liguori, A.; Sindona, G.; Uccella, N. *J. Am. Chem. Soc.* **1990**, *112*, 9092. (d) Kurinovich, M. A.; Phillips, L. M.; Sharma, S.; Lee, J. K. *Chem. Commun.* **2002**, 2354–2355.

(8) (a) Podolyan, Y.; Gorb, L.; Leszczynski, J. *J. Phys. Chem. A* **2000**, *104*, 7346. (b) Chandra, A. K.; Nguyen, M. T.; Zeegers-Huyskens, T. *J. Phys. Chem. A* **1998**, *102*, 6010. (c) Chandra, A. K.; Nguyen, M. T.; Uchimaru, T.; Zeegers-Huyskens, T. *J. Phys. Chem. A* **1999**, *103*, 8853.

(9) Wolken, J. K.; Turecek, F. *J. Am. Soc. Mass Spectrom.* **2000**, *11*, 1065.

(10) (a) Jones, W.; Boissel, P.; Chiavarino, B.; Crestoni, M. E.; Fornarini, S.; Lemaire, J.; Maitre, P. *Angew. Chem., Int. Ed.* **2003**, *42*, 2057. (b) Simon, A.; Jones, W.; Ortega, J. M.; Boissel, P.; Lemaire, J.; Maitre, P. *J. Am. Chem. Soc.* **2004**, *126*, 11666. (c) Reinhard, B. M.; Lagutschenkov, A.; Lemaire, J.; Maitre, P.; Boissel, P.; Niedner-Schatteburg, G. *J. Phys. Chem. A* **2004**, *108*, 3350. (d) Kapota, C.; Lemaire, J.; Maitre, P.; Ohanessian, G. *J. Am. Chem. Soc.* **2004**, *126*, 1836. (e) MacAleese, L.; Simon, A.; McMahon, T. B.; Ortega, J. M.; Scuderi, D.; Lemaire, J.; Maitre, P. *Int. J. Mass Spectrom.* **2006**, *249*, 14. (f) Simon, A.; MacAleese, L.; Maitre, P.; Lemaire, J.; McMahon, T. B. *J. Am. Chem. Soc.* **2007**, *129*, 2829.

(11) Bakker, J. M.; Besson, T.; Lemaire, J.; Scuderi, D.; Maitre, P. *J. Phys. Chem. A* **2007**, *111*, 13415.

(12) (a) Moore, D. T.; Oomens, J.; Eyler, J. R.; Meijer, G.; von Helden, G.; Ridge, D. P. *J. Am. Chem. Soc.* **2004**, *126*, 14726. (b) Moore, D. T.; Oomens, J.; van der Meer, L.; von Helden, G.; Meijer, G.; Valle, J.; Marshall, A. G.; Eyler, J. R. *ChemPhysChem* **2004**, *5*, 740. (c) Oomens, J.; Moore, D. T.; von Helden, G.; Meijer, G.; Dunbar, R. C. *J. Am. Chem. Soc.* **2004**, *126*, 724. (d) Valle, J. J.; Eyler, J. R.; Oomens, J.; Moore, D. T.; van der Meer, A. F. G.; von Helden, G.; Meijer, G.; Hendrickson, C. L.; Marshall, A. G.; Blakney, G. T. *Rev. Sci. Instrum.* **2005**, *76*, 023103. (e) Dunbar, R. C.; Moore, D. T.; Oomens, J. *J. Phys. Chem. A* **2006**, *110*, 8316. (f) Polfer, N. C.; Oomens, J.; Moore, D. T.; von Helden, G.; Meijer, G.; Dunbar, R. C. *J. Am. Chem. Soc.* **2006**, *128*, 517.

(13) Salpin, J. Y.; Guillaumont, S.; Tortajada, J.; MacAleese, L.; Lemaire, J.; Maitre, P. *ChemPhysChem* **2007**, *8*, 2235.

(14) Prazeres, R.; Glotin, F.; Insa, C.; Jaroszynski, D. A.; Ortega, J. M. *Eur. Phys. J. D* **1998**, *3*, 87.

(15) Frisch, M. J.; Trucks, G. W.; Schlegel, H. B.; Scuseria, G. E.; Robb, M. A.; Cheeseman, J. R.; Montgomery, J. A., Jr.; Vreven, T.; Kudin, K. N.; Burant, J. C.; Millam, J. M.; Iyengar, S. S.; Tomasi, J.; Barone, V.; Mennucci, B.; Cossi, M.; Scalmani, G.; Rega, N.; Petersson, G. A.;

Nakatsuji, H.; Hada, M.; Ehara, M.; Toyota, K.; Fukuda, R.; Hasegawa, J.; Ishida, M.; Nakajima, T.; Honda, Y.; Kitao, O.; Nakai, H.; Klene, M.; Li, X.; Knox, J. E.; Hratchian, H. P.; Cross, J. B.; Bakken, V.; Adamo, C.; Jaramillo, J.; Gomperts, R.; Stratmann, R. E.; Yazyev, O.; Austin, A. J.; Cammi, R.; Pomelli, C.; Ochterski, J. W.; Ayala, P. Y.; Morokuma, K.; Voth, G. A.; Salvador, P.; Dannenberg, J. J.; Zakrzewski, V. G.; Dapprich, S.; Daniels, A. D.; Strain, M. C.; Farkas, O.; Malick, D. K.; Rabuck, A. D.; Raghavachari, K.; Foresman, J. B.; Ortiz, J. V.; Cui, Q.; Baboul, A. G.; Clifford, S.; Cioslowski, J.; Stefanov, B. B.; Liu, G.; Liashenko, A.; Piskorz, P.; Komaromi, I.; Martin, R. L.; Fox, D. J.; Keith, T.; Al-Laham, M. A.; Peng, C. Y.; Nanayakkara, A.; Challacombe, M.; Gill, P. M. W.; Johnson, B.; Chen, W.; Wong, M. W.; Gonzalez, C.; Pople, J. A. Gaussian Program Suite. In *Gaussian 03*; Gaussian, Inc.: Wallingford, CT, 2004.

(16) Lemaire, J.; Boissel, P.; Heninger, M.; Mauclaire, G.; Bellec, G.; Mestdagh, H.; Simon, A.; Caer, S. L.; Ortega, J. M.; Glotin, F.; Maitre, P. *Phys. Rev. Lett.* **2002**, *89*, 273002.

(17) Wu, R.; McMahon, T. B. *J. Am. Chem. Soc.* **2007**, *129*, 569.

(18) NIST Chemistry WebBook, NIST Standard Reference Database Number 69; Lindstrom, P. J., Mallard, W. G., Eds.; June 2005 release.

(19) Wang, Y. S.; Chang, H. C.; Jiang, J. C.; Lin, S. H.; Lee, Y. T.; Chang, H. C. *J. Am. Chem. Soc.* **1998**, *120*, 8777.

(20) Kamariotis, A.; Boyarkin, O. V.; Mercier, S. R.; Beck, R. D.; Bush, M. F.; Williams, E. R.; Rizzo, T. R. *J. Am. Chem. Soc.* **2006**, *128*, 905.

(21) Pankewitz, T.; Lagutschenkov, A.; Niedner-Schatteburg, G.; Xantheas, S. S.; Lee, Y. T. *J. Chem. Phys.* **2007**, *126*, 074307.

(22) Mourgues, P.; Chamot-Rooke, J.; van der Rest, G.; Nedev, H.; Audier, H. E.; McMahon, T. B. *Int. J. Mass Spectrom. Ion Processes* **2001**, *210/211*, 429.

(23) (a) Stearns, J. A.; Boyarkin, O. V.; Rizzo, T. R. *J. Am. Chem. Soc.* **2007**, *129*, 13820. (b) Stearns, J. A.; Guidi, M.; Boyarkin, O. V.; Rizzo, T. R. *J. Chem. Phys.* **2007**, *127*, 154322. (c) Stearns, J. A.; Mercier, S.; Seaiby, C.; Guidi, M.; Boyarkin, O. V.; Rizzo, T. R. *J. Am. Chem. Soc.* **2007**, *129*, 11814.

(24) Elliot, B. M.; Relph, R. A.; Roscioli, J. R.; Bopp, J. C.; Gardenier, G. H.; Guasco, T. L.; Johnson, M. A. *J. Chem. Phys.* **2008**, in press.

(25) (a) Hammer, N. I.; Diken, E. G.; Roscioli, J. R.; Johnson, M. A.; Myshakin, E. M.; Jordan, K. D.; McCoy, A. B.; Huang, X.; Bowman, J. M.; Carter, S. *J. Chem. Phys.* **2005**, *122*, 244301. (b) Douberly, G. E.; Ricks, A. M.; Ticknor, B. W.; Duncan, M. A. *Phys. Chem. Chem. Phys.* **2008**, *10*, 77.

(26) Asvany, O.; Kumar, P.; Redlich, B.; Hegemann, I.; Schlemmer, S.; Marx, D. *Science* **2005**, *309*, 1219.

(27) Sinha, R.; Maitre, P. Manuscript in preparation, 2008.

JP806396T